Propagation of Light Beams in Photorefractive Media: Fanning, Self-Bending, and Formation of Self-Pumped Four-Wave-Mixing Phase Conjugation Geometries

A. A. Zozulya, M. Saffman, and D. Z. Anderson

Joint Institute for Laboratory Astrophysics, University of Colorado, C.B. 440, Boulder, Colorado 80309-0440

(Received 1 February 1994)

We investigate propagation of light beams in photorefractive media by direct numerical simulation. The two dimensional model is based on solution of nonlinear material equations and parabolic equations for the electromagnetic field. We show that this set of equations describes the wealth of complicated spatial structures observed in these media. We present results on fanning of a single beam and on formation of various four-wave-mixing geometries including self-conjugation of a light beam via total internal reflection, mutual phase conjugation, and self-bending of two counterpropagating beams.

PACS numbers: 42.65.Hw, 42.50.Ne

Propagation of laser light in a photorefractive medium is accompanied by a series of dramatic and fascinating changes of its spatial structure. Among these are the asymmetric light-induced stimulated scattering (fanning [1]) and formation of spatial distributions of the electromagnetic fields resulting in self-pumped phase conjugation and mutual conjugation of light beams incident on a photorefractive crystal [2–5]. A considerable effort went into development of various theoretical models describing these phenomena (see, e.g., reviews [6,7] and references therein). Previous analyses resulted in insight into many features of the nonlinear interaction of light with photorefractive media. But due to the complexity of the processes under investigation previous work frequently relied on *ad hoc* assumptions about the spatial structure of the electromagnetic radiation inside the medium. The aim of the present paper is to investigate formation of complex spatial structures of the electromagnetic fields in a photorefractive medium numerically, from first principles, making as few approximations as possible. We specify only the input amplitude distributions of the light beams incident on the medium. Their evolution inside the medium is governed by diffraction and material nonlinearity. The resultant distribution of the fields inside the crystal, depending on mutual orientation of the beam and the crystal faces, corresponds to the formation of one or the other spatial structures of the fields responsible for incoherent scattering or above mentioned phase conjugation or mutual conjugation geometries.

We base our analysis of the photorefractive material response on the set of equations [8]:

$$\frac{\partial}{\partial t} N_D^+ = sI(N_D - N_D^+) - \xi n_e N_D^+ , \tag{1a}$$

$$\nabla \cdot \epsilon \mathbf{E} = e(N_D^+ - N_A - n_e), \tag{1b}$$

$$\nabla \cdot \left(\epsilon \frac{\partial}{\partial t} \mathbf{E} + e\mu n_e \mathbf{E} + \kappa_B T_\mu \nabla n_e \right) = 0 . \tag{1c}$$

Here N_D, N_D^+, N_A, and n_e are the density of donors, ionized donors, acceptors, and electrons, respectively, $\mathbf{E}$ is the amplitude of the static electric field, e the electron charge, ϵ the static dielectric constant, ξ the recombination constant, μ the mobility, κ_B Boltzmann's constant, T the temperature, s the photoexcitation coefficient, and I the intensity of electromagnetic radiation plus equivalent dark intensity connected with thermal excitation of charge carriers. Assume that all functions in Eqs. (1) predominantly change along the y direction, and so all differential operators are replaced by a partial derivative along this direction. In steady state ($\partial/\partial t = 0$) and under the standard assumptions of $N_D \gg N_A$, and fast carrier recombination, Eqs. (1) may be reduced to one equation for the normalized amplitude of the static electric field $\nu = E/\tilde{E}$, where $\tilde{E} = \kappa_B T k_D / e \equiv e N_A / \epsilon k_D$ and where $k_D = (e^2 N_A / \kappa_B T \epsilon)^{1/2}$ is the characteristic Debye wave number:

$$\nu - \frac{1}{(k_D)^2} \frac{\partial^2 \nu}{\partial y^2} \left(1 + \frac{1}{k_D} \frac{\partial \nu}{\partial y} \right)^{-1} = -\frac{1}{k_D} \frac{\partial}{\partial y} \ln I . \tag{2}$$

The equations governing propagation of the optical fields have the form

$$\left(\frac{\partial}{\partial x} - \frac{i}{2k} \frac{\partial^2}{\partial y^2} \right) A_f = 2i\gamma_0 \nu A_f , \tag{3a}$$

$$\left(-\frac{\partial}{\partial x} - \frac{i}{2k} \frac{\partial^2}{\partial y^2} \right) A_b = 2i\gamma_0 \nu A_b , \tag{3b}$$

where k is the wave number of electromagnetic radiation inside the medium and A_f and A_b are forward and backward propagating electromagnetic fields, respectively. Equations (3) are written in the paraxial approximation; i.e., the angles of propagation of all beams with respect to the x axis are assumed to be small as compared to unity. The same paraxial approximation ensures that all functions in Eqs. (1) predominantly change along the y direction. Values of the appropriate components of the electro-optic tensor that give the relation between the static electric field ν and the nonlinear refractive index change are lumped into the nonlinearity constant γ_0.

0031-9007/94/73(6)/818(4)$06.00

The angular dependence of the electro-optic tensor is neglected as compared to that given by Eq. (2). The intensity of the electromagnetic radiation I in Eq. (2) is equal to the sum of the beam intensities, plus an equivalent dark intensity connected with dark conductivity or (possible) incoherent erasure intensity: $I = |A_f|^2 + |A_b|^2 + I_{er}$. In the following we shall use, instead of the Debye wave number k_D, the Debye angle θ_D, determined by the relation $\theta_D = k_D/k$. If the medium is illuminated by two plane waves $A_f = A_1 + A_2$ ($|A_1| \ll |A_2|$), propagating at an angle θ to each other, the weak wave A_1 grows exponentially in space ($A_1 \sim \exp[\gamma(\theta)x]$) from its boundary value with the growth rate [8]:

$$\gamma(\theta) = \gamma_0 \frac{2(\theta/\theta_D)}{1 + (\theta/\theta_D)^2}. \quad (4)$$

The angle θ_D is thus the angle between plane wave pump and signal beams corresponding to the maximum coupling between them, and γ_0 is the value of this coupling. The boundary conditions for the system of Eqs. (2) and (3) correspond to specification of input amplitude distributions of the forward and backward propagating beams $A_{f,\text{in}}(y)$, $A_{b,\text{in}}(y)$. The system of Eqs. (2) and (3) is the same as that used in recent papers [9,10], but we concentrate here on different topics. Equations (3) were solved using a finite difference Crank-Nicholson type scheme [11]. Equation (2) was solved by relaxation methods. Solution of Eqs. (2) and (3) is an initial-value problem, and is less computationally demanding, when considering fanning of a single beam. These calculations were carried out for values of the parameters corresponding to experimental ones. The presence of feedback in the case of formation of phase conjugation geometries makes it a boundary-value problem, requiring larger resources. These calculations were carried out with downscaled values of the experimental parameters (diameters of the beams and size of the computation region).

We found that efficient development of all the above mentioned spatial structures of the electromagnetic field requires, besides nonlinearity, the presence of a sufficiently large background of spatially broadband radiation (noise) that serves as seeds for generating these structures. These seeds may be due to surface and volume scattering in the nonlinear medium or they may be present in the input beam if its spatial spectrum is broad enough. We do not consider volume scattering in this paper, and all background seeds are added to the input beams.

Figure 1(a) shows a typical picture of asymmetric incoherent stimulated photorefractive scattering (fanning) of a single light beam. The sizes of the computation region are $l_x = 5$ mm, $l_y = 2$ mm along coordinates x and y, respectively, and the beam propagates at an angle $\theta = -6°$ to the x axis. The number of transverse points used in the calculations was 12 000 (corresponding to $\approx 72°$) and the number of longitudinal steps was 3000. The input and the output intensity distributions of the beam are shown in Fig. 1(b). The beam is a Gaussian with diameter $d = 0.3$ mm with superimposed noise. The power spectrum of this noise has a Gaussian envelope with FWHM $\approx 12°$. The ratio of maximum spectral intensity of the noise to that of the Gaussian kernel is about 10^{-4}. The total power in the low-intensity noise pedestal is about 0.01 of that of the Gaussian kernel. The nonlinearity $\gamma_0 l_x = 12$ and $\theta_D = 8°$. Figure 1(a) demonstrates that the beam breaks down into a fan of narrow filaments. This picture is in very good agreement with experimental observations.

Figure 2 shows the spatial structure of the fields corresponding to the geometry of a total internal reflection phase conjugator [2]. As is shown in Ref. [2] the incident beam is aligned in such a way that its fanning is directed towards a corner of the crystal that acts as a retroreflector. The reflected fanning couples nonlinearly with the input beam, finally forming a loop structure. The resulting backpropagating beam is a phase conjugate replica of the incident beam. The input beam for these calculations is similar to that used in the calculations of fanning. It has a Gaussian kernel with superimposed random modulation. The power spectrum of this modulation has a Gaussian envelope with FWHM $\approx 9°$ and with relative peak intensity

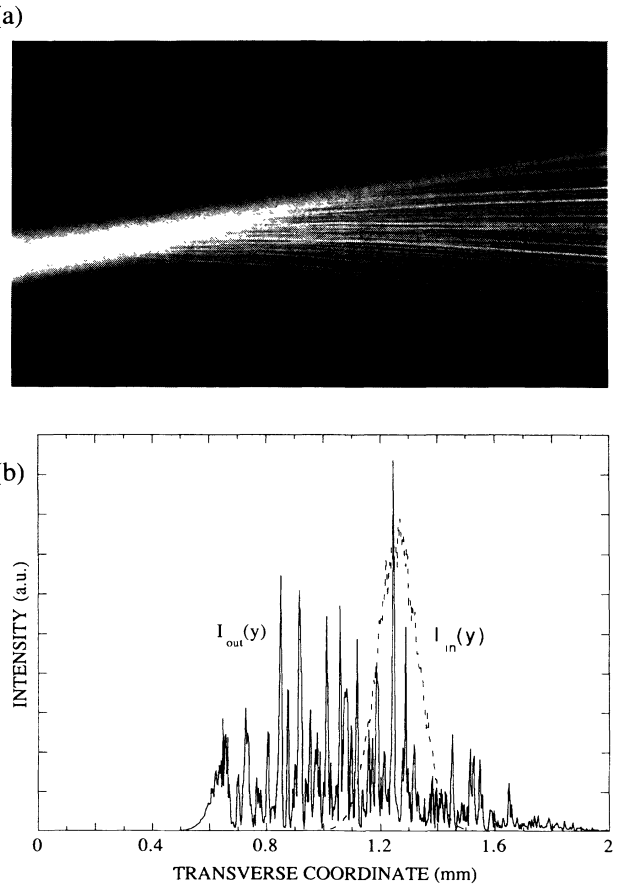

FIG. 1. Fanning of a beam in a photorefractive medium: (a) distribution of light intensity inside the crystal for $\gamma_0 l_x = 12$, (b) intensity profiles of the input (dashed) and the output (solid) radiation.

$\approx 2 \times 10^{-3}$. The beam has diameter $d = 0.06$ mm and propagates at an angle $\theta = 1°$ to the x axis. The size of the computation region is $l_x = 1$ mm, $l_y = 0.2$ mm, $\gamma_0 l_x = 13$, and $\theta_D = 8°$. Calculations were carried out on a 500 (along x) $\times$ 1000 (along y) grid. Reflection from crystal faces was described phenomenologically. The radiation incident at the back crystal face was decomposed into Fourier harmonics. Those incident at angles less than 10° were transmitted; the rest were totally reflected. The side faces are ideally reflecting. The input (dashed) and the output (solid) intensity distributions of the beam are shown in Fig. 2(b), which demonstrates reproduction of the beam input structure and shows that the output beam is a reasonable phase conjugate replica of the input one. The nonlinear reflectivity R and the conjugation fidelity H (as defined in [10]) for Fig. 2 are equal to $R \approx 0.87$ and $H \approx 0.85$.

Figure 3 demonstrates phase conjugation of two almost counterpropagating light beams [3,4]. Figure 3(a) shows the rhomboid-shaped beam overlap region in the absence of nonlinearity, Fig. 3(b) corresponds to $\gamma_0 l_x = 11$, and Fig. 3(c) to $\gamma_0 l_x = 15$. The nonlinearity causes the beams to form a distributed region of shared refractive index gratings, and to bend smoothly into each other, producing backpropagating phase conjugate beams. The effect of smooth self-bending is especially striking when compared

(a)

(b)

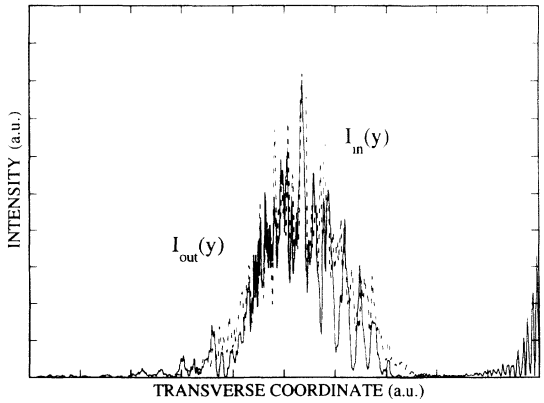

FIG. 2. Structure of fields in the geometry of a total internal reflection phase conjugate mirror: (a) distribution of light intensity inside the crystal and (b) input (dashed) and output (solid) intensity profiles of the beam.

(a)

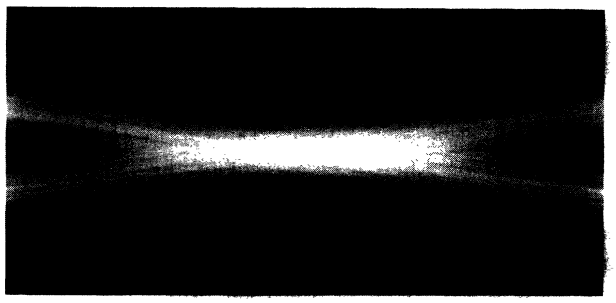

(b)

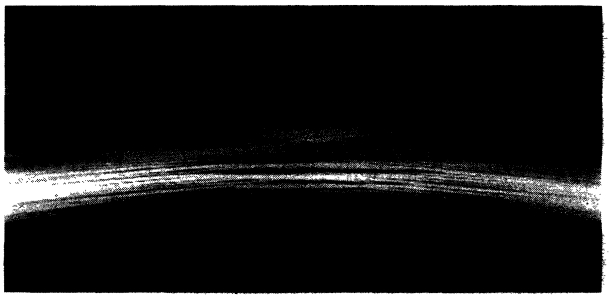

(c)

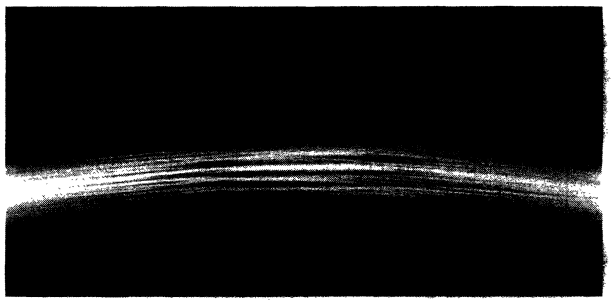

FIG. 3. Structure of fields corresponding to mutual phase conjugation and bending of two light beams: (a) distribution of light intensity in the crystal for $\gamma_0 l_x = 0$, (b) the same for $\gamma_0 l_x = 11$, and (c) the same for $\gamma_0 l_x = 15$.

to what happens to a single beam [Fig. 1(a)]. Figure 4 gives intensity distributions of the input and output radiation at one of the faces of the crystal (the fields at the second face look very similar), for $\gamma_0 l_x = 11$ [(a)] and 15 [(b)]. Dashed curves are the input fields and solid curves the output ones. The intensity hump on the left sides of Figs. 4(a) and 4(b) corresponds to the part of the incident beams that passed through the nonlinear medium without interaction. Its relative magnitude diminishes with the increase of nonlinearity. The overlapping parts of the dashed and the solid curves on the right sides of Figs. 4(a) and 4(b) correspond to generation of phase conjugate radiation. Notice the spatial shift of the phase conjugate beams with respect to the counterpropagating input beams. The shift is clearly seen in Fig. 4(a), corresponding to a lower nonlinearity, and is almost nonexistent in Fig. 4(b). Its physical origin was

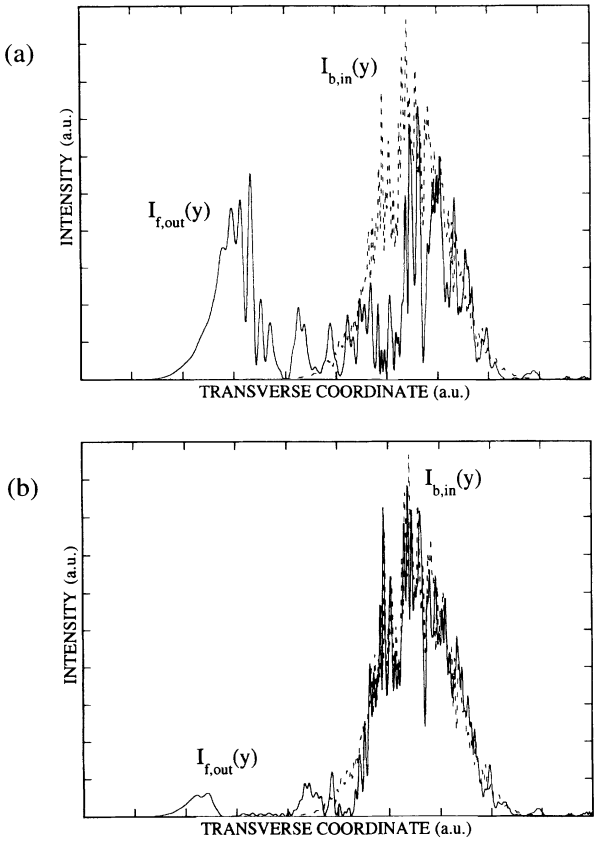

FIG. 4. Input and output intensity distributions of the beams at the left face of the crystal for the geometry of Fig. 3 for (a) $\gamma_0 l_x = 11$ and (b) $\gamma_0 l_x = 15$.

discussed in [7]. The nonlinear reflectivities and conjugation fidelities are equal to $R \approx 0.6$, $H \approx 0.5$ for Figs. 3(b) [4(a)] and $R \approx 0.9$, $H \approx 0.9$ for Figs. 3(c) [4(b)]. The size of the computation region for Figs. 3 and 4 is 1.2 mm $\times$ 0.3 mm (600 $\times$ 1250 points); the beams have the same powers and diameters $d = 0.08$ mm and intersect in the medium at an angle $\theta = 8°$. The spatial spectrum of the input fields is similar to that used in the previously discussed calculations and, finally, $\theta_D = 8°$.

Figure 5 shows two equal power beams with the same diameter $d = 0.06$ mm intersecting in a photorefractive medium at an angle $\theta = 6°$. The rhomboid-shaped beam overlap region in the absence of nonlinearity lies just above the side face of the crystal that is ideally reflecting. The direction of fanning is toward the face. It is the closeness of this reflecting face to the beam overlap region that makes the situation different from that of Figs. 3 and 4. The beams fan toward the face, and the fanning of each beam after having been reflected from the face

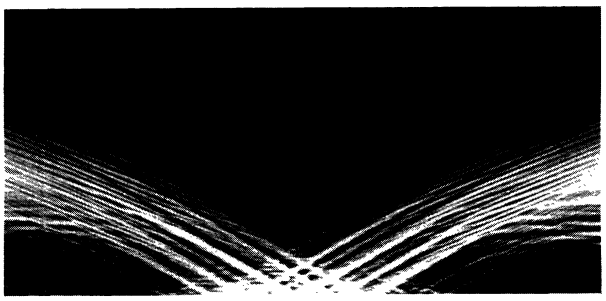

FIG. 5. Structure of the fields corresponding to mutual phase conjugation and bending of two light beams coupled via a reflecting crystal face (the bird wing geometry).

intersects the other. The result is mutual self-bending and phase conjugation of the beams, with the formation of a very characteristic bird wing structure [5]. The size of the computation region for this picture is 1 mm $\times$ 0.12 mm (500 $\times$ 1000 points), $\gamma_0 l_x = 15$, and $\theta_D = 8°$. The nonlinear reflectivities and the conjugation fidelities are equal to about 0.8 and 0.5, respectively.

In conclusion, we investigated numerically the two dimensional propagation of a light beam in a nonlinear photorefractive medium by direct "first principles" numerical simulation. The two dimensional model was based on solution of nonlinear material equations and parabolic equations for electromagnetic radiation. We have demonstrated for the first time how this model, in a unified way, describes the formation of complex spatial structures when light beams propagate inside these media.

This work was supported by NSF Grant No. PHY90-12244.

[1] V. V. Voronov *et al.*, Sov. J. Quantum Electron. **10**, 1346 (1980).
[2] J. Feinberg, Opt. Lett. **7**, 486 (1982).
[3] S. Weiss, S. Sternklar, and B. Fischer, Opt. Lett. **12**, 114 (1987).
[4] D. Wang *et al.*, Opt. Commun. **73**, 495 (1989).
[5] M. D. Ewbank, Opt. Lett. **13**, 47 (1987).
[6] M. Cronin-Golomb *et al.*, IEEE J. Quantum Electron. **20**, 12 (1984).
[7] V. T. Tikhonchuk and A. A. Zozulya, Prog. Quantum Electron. **15**, 231 (1991).
[8] N. V. Kukhtarev *et al.*, Ferroelectrics **22**, 949 (1979).
[9] M. Cronin-Golomb, Opt. Commun. **89**, 276 (1992).
[10] A. A. Zozulya, M. Saffman, and D. Z. Anderson, "Double phase conjugate mirror: convection and diffraction" (to be published).
[11] L. Sun and G. L. Yip, Opt. Lett. **18**, 1229 (1993).

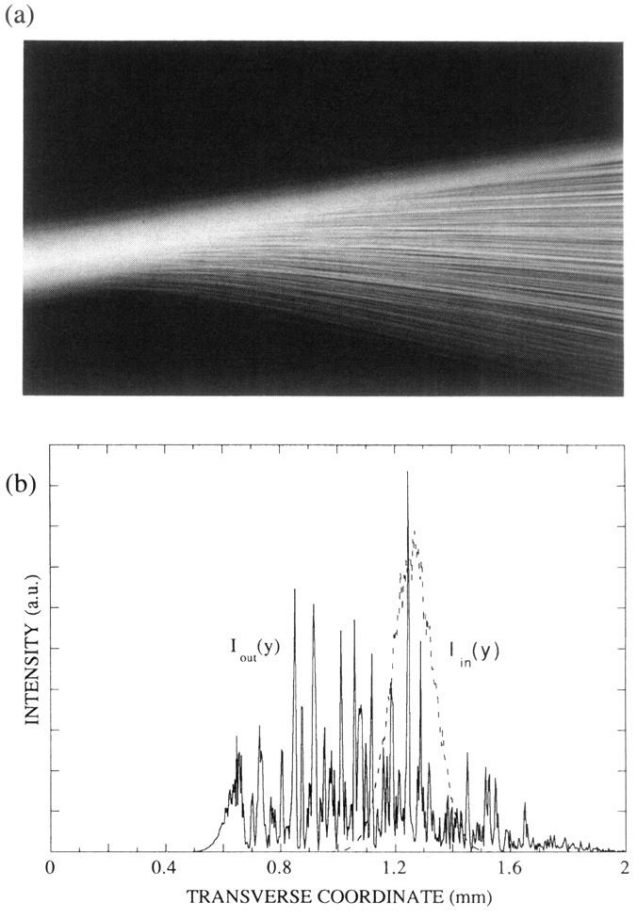

FIG. 1. Fanning of a beam in a photorefractive medium: (a) distribution of light intensity inside the crystal for $\gamma_0 l_x = 12$, (b) intensity profiles of the input (dashed) and the output (solid) radiation.

(a)

(b)

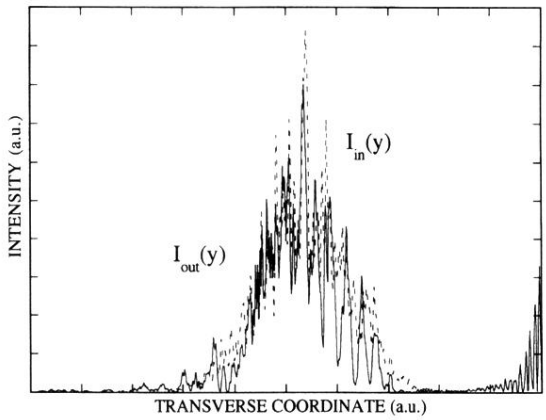

FIG. 2. Structure of fields in the geometry of a total internal reflection phase conjugate mirror: (a) distribution of light intensity inside the crystal and (b) input (dashed) and output (solid) intensity profiles of the beam.

(a)

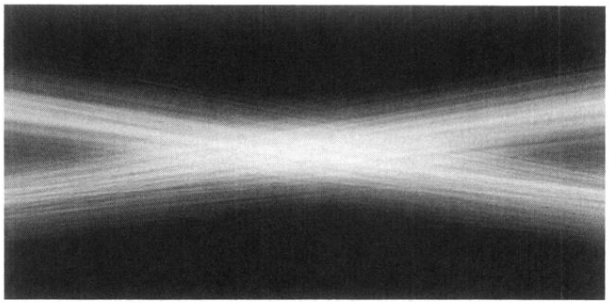

(b)

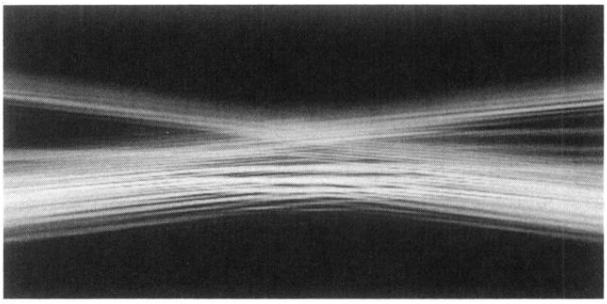

(c)

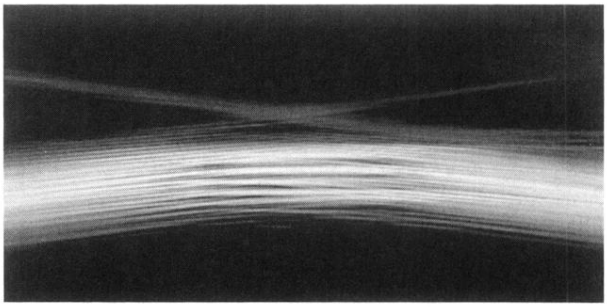

FIG. 3. Structure of fields corresponding to mutual phase conjugation and bending of two light beams: (a) distribution of light intensity in the crystal for $\gamma_0 l_x = 0$, (b) the same for $\gamma_0 l_x = 11$, and (c) the same for $\gamma_0 l_x = 15$.

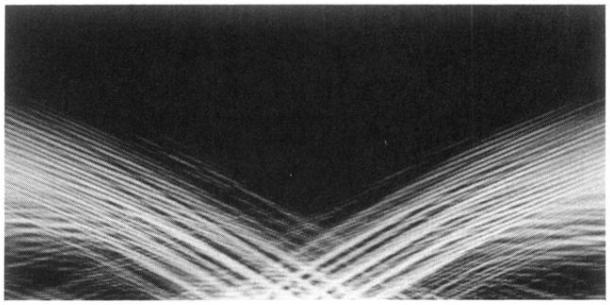

FIG. 5. Structure of the fields corresponding to mutual phase conjugation and bending of two light beams coupled via a reflecting crystal face (the bird wing geometry).